Available online at www.sciencedirect.com

ScienceDirect

Proceedings of the Combustion Institute 37 (2019) 4519–4529

Proceedings of the Combustion Institute

www.elsevier.com/locate/proci

Large Eddy Simulation of MILD combustion using finite rate chemistry: Effect of combustion sub-grid closure

Zhiyi Li [a,b,*], Alberto Cuoci [c], Alessandro Parente [a,b]

[a] *Université Libre de Bruxelles, Ecole polytechnique de Bruxelles, Aero-Thermo-Mechanics Laboratory, Bruxelles, Belgium*
[b] *Université Libre de Bruxelles and Vrije Universiteit Brussel, Combustion and Robust Optimization Group (BURN), Brussels, Belgium*
[c] *Department of Chemistry, Materials, and Chemical Engineering, Politecnico di Milano, P.zza Leonardo da Vinci, Milano 20133, Italy*

Received 30 November 2017; accepted 18 September 2018
Available online 19 October 2018

Abstract

In this work, we present a detailed comparison between the conventional Partially Stirred Reactor (PaSR) combustion model and two implicit combustion models, named Quasi Laminar Finite Rate (QLFR) model and Laminar Finite Rate (LFR) model, respectively. Large Eddy Simulation (LES) is employed and the Adelaide Jet in Hot Co-flow (AJHC) burner is chosen as validation case. In the implicit combustion models, the filtered source term comes directly from the chemical term, without inclusion of turbulence effects. Results demonstrate that the two implicit models behave similarly to the conventional PaSR model, for the mean and root-mean-square of the temperature and species mass fractions, and that all models provide very satisfactory predictions, especially for the mean values. This justifies the use of implicit combustion models in low Damköhler number (Da $\leq$ 1.0) systems. The QLFR model allows to reduce the computational cost of about three times, compared to the LFR model. Moreover, the comparison between two 4-step global mechanisms and the KEE58 mechanism proves the importance of finite rate chemistry in MILD combustion.

Keywords: Adelaide JHC burner; Detailed chemistry; MILD combustion; Implicit combustion models; Partially Stirred Reactor; Subgrid combustion models

1. Introduction

Moderate or Intense Low oxygen Dilution (MILD) combustion has the advantages of uniformly distributed temperature field, reduced NO_x and soot formation, as well as higher fuel flexi-

* Corresponding author at: Université Libre de Bruxelles, Ecole polytechnique de Bruxelles, Aero-Thermo-Mechanics Laboratory, Bruxelles, Belgium.
E-mail addresses: Zhiyi.Li@ulb.ac.be (Z. Li), Alessandro.Parente@ulb.ac.be (A. Parente).

https://doi.org/10.1016/j.proci.2018.09.033

bility compared to conventional combustion technologies [1,2]. In MILD combustion, reaction can occur over a wide range of turbulence scales, instead of the smallest scale in conventional combustion [3]. The system evolves towards a distributed reaction regime and low temperatures, because of the high dilution level and the intense mixing between reactants and combustion products. This leads to higher chemical and lower mixing time scales, thus to characteristic Damköhler number of order ~ 1 [1,2]. As a result, combustion progress in such systems cannot be described using models based on the principle of time scale separation [4], and approaches accounting for finite rate chemistry should be considered. In the present paper, the Partially Stirred Reactor (PaSR) model [5] is considered. In PaSR, the influence of the sub-grid fluctuations on the reaction rate is expressed with a factor κ, defined as the ratio between the characteristic chemical time scale and the sum of the chemical and mixing time scales. Recently, it was shown that κ approaches 1 in MILD combustion, suggesting that reacting structures can be fully resolved on the Large Eddy Simulation (LES) grid using a laminar finite rate model [6].

Successful predictions of MILD systems are reported in the literature. Many contributions refer to lifted jet flames in vitiated co-flow [7], for which several investigations have been carried out using Reynolds Averaged Navier–Stokes (RANS) simulation. In the context of RANS simulation, different authors focused on the over-prediction of temperature obtained using standard EDC constants. Adjusted EDC constants [8,9], based on a fitting procedure, were used to alleviate the over-predicted temperature. Parente et al. [10] proposed a dynamic expression of the EDC constants based on local values of turbulent Reynolds number Re_T and Damköhler number, Da, proving the importance of considering the chemical time scale in MILD combustion. However, despite the computational efficiency of RANS simulations, they are not able to capture non-equilibrium phenomena, such as local extinction and re-ignition. On the other end, Large Eddy Simulation (LES) can resolve the unsteady flow structure and reproduce turbulence with a much higher accuracy than RANS. Ihme et al. [11,12] carried out LES on the Adelaide Jet in Hot Co-flow (AJHC) burner using a three-stream Flamelet Progress Variable (FPV) formulation. Good agreement with the experimental measurements was observed for the mean temperature and specie mass fraction profiles. Afarin et al. [13] used PaSR to investigate the reaction zone structure as well as the distribution of temperature and minor species mass fractions, showing satisfactory accuracy.

The present paper focuses on the applicability of different implicit combustion model formulations, under MILD combustion conditions. The PaSR model is benchmarked against two implicit formulations, the Laminar Finite Rate (LFR) and the Quasi-Laminar Finite Rate (QLFR) formulations. In the LFR model, the mean source term is directly retrieved from the Arrhenius expression, while in the QLFR model, a time-splitting approach is used, solving an Ordinary Differential Equation (ODE) to describe the evolution of species mass fractions within the LES residence time. The AJHC burner [7] is chosen as the test case, as it provides high-fidelity measurements of mean and root-mean-square (rms) temperature, mixture fraction, and species mass fraction for a MILD combustion prototype system. All simulations are carried out using OpenFOAM, where the different models (PaSR, QLFR and LFR) are implemented [10,14]. Finite rate chemistry and multi-component molecular species diffusion are included in the calculation. The assessment of the model performances is based on both the mean and variance of the temperature and species mass fraction profiles.

2. Numerical models

2.1. Turbulence model

The one equation eddy viscosity (`oneEqnEddy`) is chosen as sub-grid turbulence model [15]. The Favre-filtered governing equations of continuity, momentum, energy and species are solved. The sub-grid stress tensor for the Favre-filtered momentum field, expressed as

$$\overline{\tau_{ij}} = \rho\widetilde{u_i u_j} - \rho\tilde{u}_i\tilde{u}_j, \tag{1}$$

requires a turbulence model. In `oneEqnEddy` model, $\overline{\tau_{ij}}$ is estimated by a subgrid-scale eddy viscosity ν_{sgs} and a resolved scale strain rate $\overline{S}_{ij}$:

$$\overline{\tau_{ij}} \approx -2\nu_{sgs}\overline{S}_{ij}. \tag{2}$$

The sub-grid scale viscosity is computed as

$$\nu_{sgs} = C_k\sqrt{k_{sgs}}\Delta, \tag{3}$$

where $C_k = 0.094$, Δ is the grid size and k_{sgs} is the sub-grid scale kinetic energy which is solved through a dedicated transport equation [16].

2.2. Combustion model

Two implicit models are compared with the conventional PaSR model. Their key model features are presented in Table 1.

2.2.1. Partially stirred reactor model

The Partially Stirred Reactor (PaSR) [5] separates each computational cell into two zones. Reaction happens only in a fraction of the cell, identified by the reacting fraction κ [17]. Thus, the mean source term can be expressed as

$$\overline{\dot{\omega}}_k = \kappa\dot{\omega}_k^*(\widetilde{\boldsymbol{Y}}, \widetilde{T}). \tag{4}$$

Table 1
Characteristics of different combustion models (scaled CPU time based on KEE58 mechanism).

Combustion model	PaSR	QLFR	LFR
Turbulence effect	Explicit	Implicit	Implicit
ODE integration	Yes	Yes	No
Detailed chemistry	Yes	Yes	Yes
Scaled CPU time	1	0.86	2.66

In Eq. (4), $\dot{\omega}_k^*(\widetilde{\boldsymbol{Y}}, \widetilde{T})$ represents the formation rate of species k based on the Favre-averaged mass fractions of species in the cell. The term κ is a coefficient which considers the non-perfect mixing, calculated as

$$\kappa = \frac{\tau_c}{\tau_c + \tau_{mix}}, \tag{5}$$

where τ_c is the characteristic chemical time scale in each cell and τ_{mix} is the mixing time scale. In the present study, the chemical time scale of each species is estimated by $\tau_{c,k} = Y_k^*/(dY_k^*/dt)$, where Y_k^* and dY_k^*/dt are mass fraction of the k_{th} species and the corresponding formation rate in the reacting zone, respectively. The highest limiting value is chosen as the characteristic chemical time scale, considering only active species (the species characterized by an absolute rate of change (dY_k^*/dt) higher than a given threshold). The mixing time scale is represented with the geometrical mean of the sub-grid velocity stretch time ($\Delta/v^{'}$) and the Kolmogorov time scale ($(\nu/\epsilon_{sgs})^{1/2}$) [18].

2.2.2. Quasi laminar finite rate model

Based on the PaSR model, the QLFR model is formulated merely by forcing $\kappa = 1.0$ [19], under the hypothesis that the mixing time scale is much smaller than the chemical time scale. Therefore, the turbulent eddies are assumed to be able to penetrate into the flame structures and the whole cell is considered as a Perfectly Stirred Reactor (PSR) [6]. Using a time-splitting approach, the reactive zone conditions are retrieved solving the following set of ODEs:

$$\frac{dY_k}{dt} = \frac{\dot{\omega}_k}{\rho}. \tag{6}$$

The term $\dot{\omega}_k$ is the instantaneous formation rate of species k. The final integration of $\frac{dY_k}{dt}$ over the residence time τ in the reactor is Y_k^* introduced in Section 2.2.1. The term $\dot{\omega}_k^*(\widetilde{\boldsymbol{Y}}, \widetilde{T})$ in Eq. (4) is thus estimated with:

$$\dot{\omega}_k^*(\widetilde{\boldsymbol{Y}}, \widetilde{T}) = (Y_k^* - \widetilde{Y}_k)/\tau. \tag{7}$$

In the present work, τ is equal to the simulation time step. As far as the CPU requirements are concerned, the QLFR model allows saving additional time compared to PaSR model, as it does not need any chemical time scale estimation for the evaluation of κ.

Table 2
Boundary conditions for the AJHC burner.

Profiles	Central jet	Annulus	Tunnel
Velocity	58.74 m/s	3.2 m/s	3.3 m/s
Temperature	294 K	1300 K	294 K

2.2.3. Laminar Finite Rate model

The Laminar Finite Rate model does not directly account for the effect of turbulence in the mean source term, and the mean formation rates are determined by Arrhenius expressions [20]:

$$\overline{\dot{\omega}}_k = M_k \sum_{r=1}^{N_r} \hat{R_{k,r}}. \tag{8}$$

In Eq. (8), M_k is the molecular weight of species k and $\hat{R_{k,r}}$ is the Arrhenius rate of creation/destruction of species k in reaction r. The LFR model is generally used for laminar reacting flows [21] or in the context of Direct Numerical Simulation (DNS). In LES applications, the LFR model is valid when the grid size is sufficiently small and the flame structure is thick enough (low Damköhler number system). It is worth mentioning that the direct coupling of source terms without a time splitting scheme imposes to use smaller time steps with respect to the one required from the PaSR and QLFR models, to ensure the simulation stability.

3. Validation test case

The Adelaide Jet in Hot Co-flow (AJHC) burner [7] emulates the MILD combustion with a simple geometry. It is thus suitable for the LES analysis.

3.1. Experimental data

The AJHC burner has a central jet with the inner diameter of 4.25 mm and an annulus pipe providing the hot co-flow with the inner diameter of 82 mm. The burner is mounted in a wind tunnel (air is used as tunnel gas), with the cross section of 254 mm × 254 mm. The central jet provides an equi-molar mixture of CH_4 and H_2. A secondary burner is mounted upstream of the annulus pipe exit plane, providing the hot combustion products which mix with air and nitrogen. The oxygen level is controlled to 3%, 6% and 9%, by adjusting the amount of air and nitrogen.

The gas temperature and velocity profiles of the central jet, annulus and wind tunnel are presented in Table 2. In this paper, the condition corresponding to a Reynolds number of 10,000 and and co-flow oxygen content of 3% is studied.

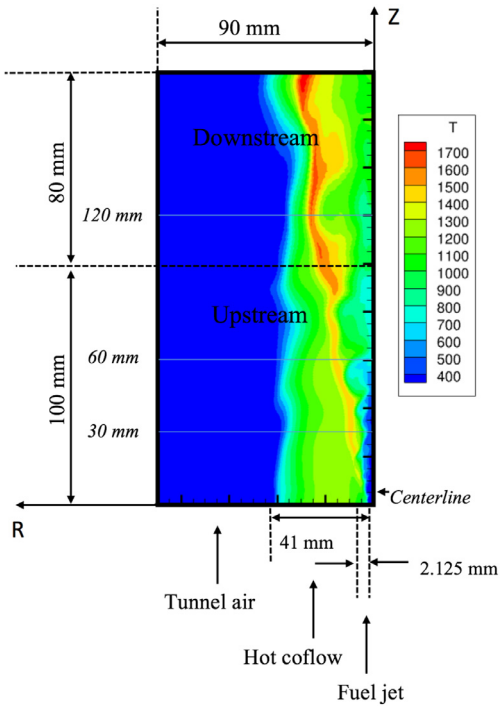

Fig. 1. 2D axi-symmetric sketch of the AJHC burner with the instantaneous temperature profile and sampling locations.

The mean and rms profiles of temperature, mixture fraction and mass fractions of species (CH_4, H_2, H_2O, CO_2, N_2, O_2, NO, CO, and OH) along the centerline as well as on the axial positions of 4/30/60/120/200 mm are available for model validation. The mean experimental measurements data shown in the validation work include the 99.99% confidence intervals as well.

3.2. Numerical set-up

The simulation domain starts from the jet exit and extends 180 mm further downstream. The radial direction expands 90 mm away from the centerline. The whole domain is discretized with a 3D cylinder structured mesh containing ~1.5 million cells. The energy resolved in the grid reaches at least 80% and more than 90% at several locations of interest, indicating a sufficient small grid size.

The LEMOS [22] inflow generation method for velocity field is applied for all the three streams. The `WaveTransmissive` [23] boundary condition is used for pressure outlet. Experimentally measured profiles (H_2O, CO_2 O_2 species mass fractions and temperature) are directly used as inflow data for the simulation. The Chapman–Enskog formulation is employed for multi-component diffusion. Three different chemical mechanisms, the 4-step global mechanism from Jones and Lindstedt (JL) [24], a modified JL mechanism from Wang et al. [25], as well as a reduced skeletal mechanism KEE58 [26] are considered. The sampling locations are the centerline and 30/60/120 mm axial locations. Both mean and variance profiles are sampled. The mean value is obtained from the time averaged instantaneous profiles. A 2D axi-symmetric sketch of the simulation domain and the sampling positions are shown in Fig. 1.

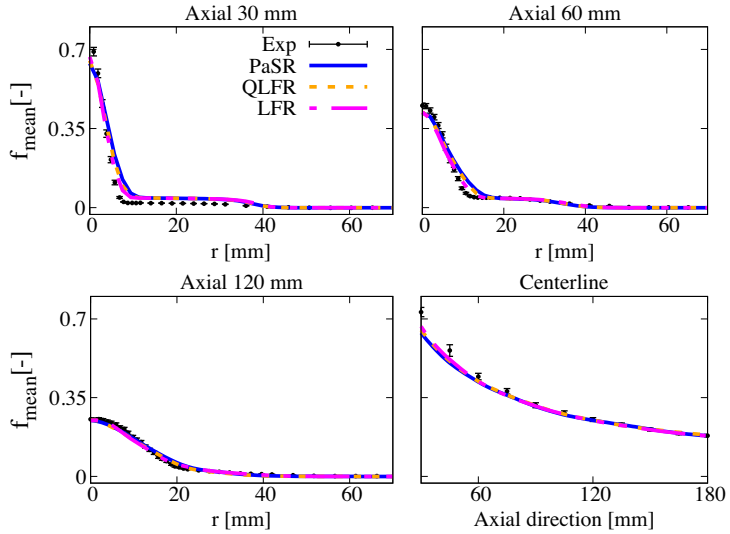

Fig. 2. Mean mixture fraction (f_{mean}) profiles obtained with the conventional PaSR model, the PaSR based QLFR model and the LFR model, at several sampling locations, compared to the experimental measurements. Kinetic mechanism: KEE58.

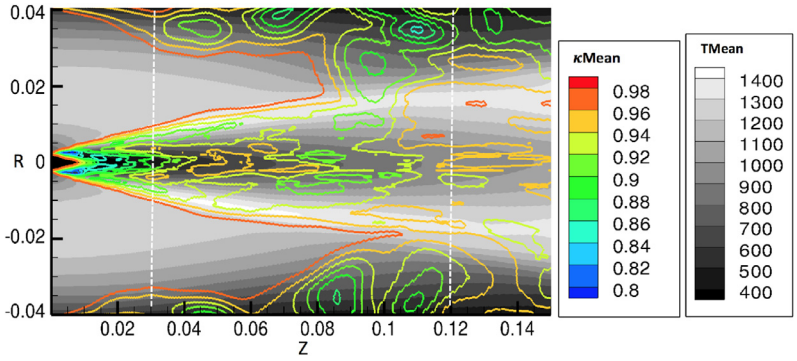

Fig. 3. Mean κ field (mean temperature in background, axis unit: m).

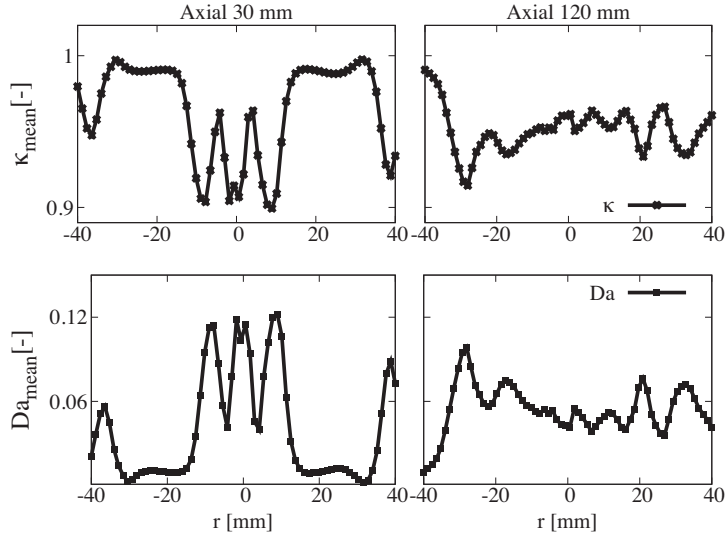

Fig. 4. Mean κ and mean Damköhler number at 30 mm and 120 mm axial locations.

4. Results and discussion

In Section 4.1, the simulation results from the two implicit combustion models are compared with the PaSR model and the experimental data. The comparison between a global and a skeletal chemistry is discussed in Section 4.2, demonstrating the importance of finite rate chemistry in MILD combustion.

4.1. Conventional and implicit combustion models

Firstly, the mixture fraction profiles provided by the three models are compared in Fig. 2, using Bilger's definition [26], to assess the ability of the different approaches to describe the mixing process. The mean mixture fractions (f_{mean}) provided by the different models are almost identical. One can conclude that the mixing field is well predicted, even though all models slightly under-predict the mean mixture fraction values close to jet exit position, for $z \leq 45$ mm.

In order to assess the possibility of using implicit combustion models, the averaged values of κ and Da, obtained with the PaSR model are analysed. In Fig. 3, the averaged κ values are shown with mean temperature profile in background. It can be observed that, in the areas where combustion takes place (from $z = 30$ mm onward), κ values are in the range from 0.9 to 1.0, indicating that most of the cell is occupied by reacting structures. In Fig. 4, the radial profiles of κ and Damköhler number are plotted at selected axial locations (30 and 120 mm). It can be observed that κ is always larger than 0.9 and Damköhler number is always smaller than 0.15 at both locations.

The mean temperature profiles provided by the three combustion models are compared to the experimental data at different sampling locations in

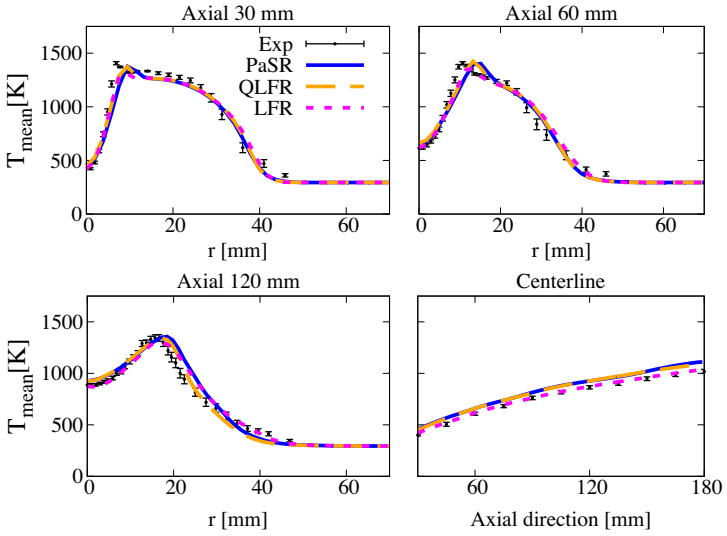

Fig. 5. Mean temperature profiles obtained with the conventional PaSR model, the PaSR based QLFR model and the LFR model, at several sampling locations, compared to the experimental measurements. Kinetic mechanism: KEE58.

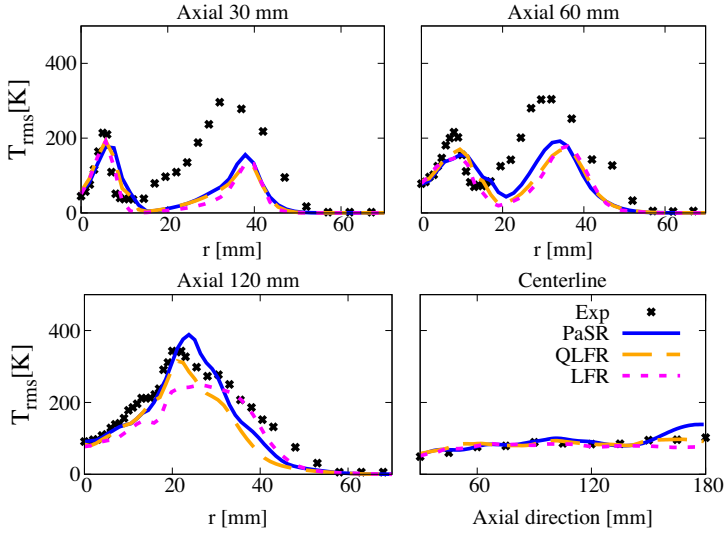

Fig. 6. Root-mean-square (rms) temperature profiles obtained with the conventional PaSR model, the PaSR based QLFR model and the LFR model, at several sampling locations, compared to the experimental measurements. Kinetic mechanism: KEE58.

Fig. 5. The temperature profiles are similar, showing only minor differences between each other and very good predictions of experimental data. At $z = 30$ mm, the LFR model underpredicts the mean temperature peak by 100 K, and the peak temperature is only slightly higher than the co-flow temperature, suggesting later ignition with respect to the other models. This is confirmed by the analysis of the OH contour plots (see Supplementary Material), showing a higher lift-off height for the LFR model. Very satisfactory agreement with the measurement data is observed at 120 mm axial location for all the three models. The QLFR model predicts the peak temperature exactly (1 K difference compared to experimentally measured mean value), while PaSR and LFR models over-predict and under-predict the value by 15 K and 40 K, respectively. Regarding the centerline profile, the later ignition predicted by LFR model corrects the slight over-prediction (around 7%) of mean temperature by the other two models. Interestingly, the results obtained with the PaSR and QLFR models are

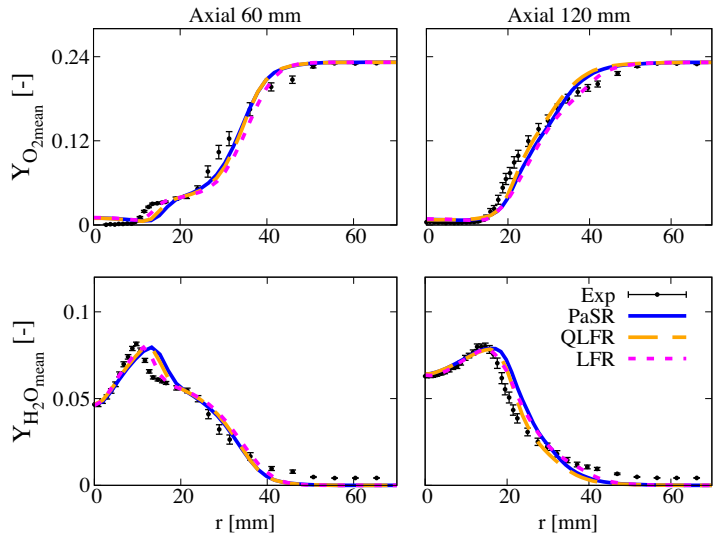

Fig. 7. Mean O_2 and H_2O mass fraction profiles obtained with the conventional PaSR model, the PaSR based QLFR model and the LFR model, at two sampling locations (z = 60 mm and z = 120 mm), compared to the experimental measurements. Kinetic mechanism: KEE58.

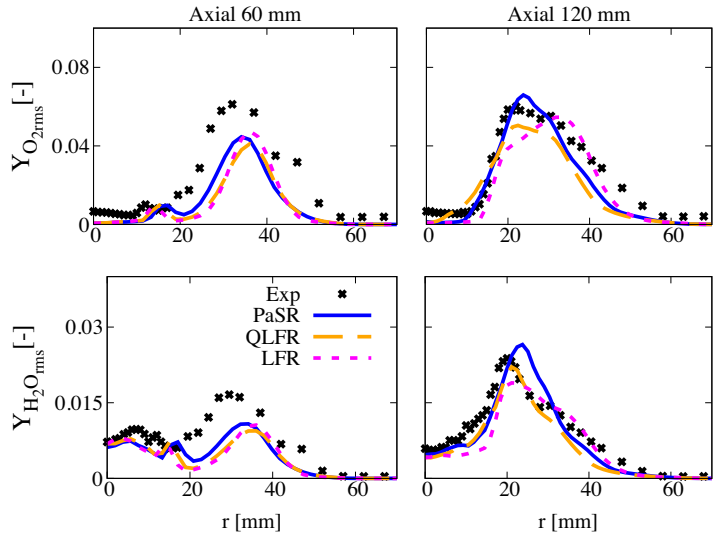

Fig. 8. Root-mean-square (rms) O_2 and H_2O mass fraction profiles obtained with the conventional PaSR model, the PaSR based QLFR model and the LFR model, at two sampling locations (z = 60 mm and z = 120 mm), compared to the experimental measurements. Kinetic mechanism: KEE58.

almost overlapping, indicating that the approximation of $\kappa = 1.0$ is appropriate and thus the assumption of an implicit closure is suitable for the investigated system. The mean profiles obtained are also similar compared to the ones presented in the research work of Ihme et al. [12]. In the present work, more accurate temperature predictions are obtained for the radial profiles at 30 mm and 60 mm downstream of the burner.

The rms value of temperature is shown in Fig. 6. The first peak at axial 30 mm and 60 mm locations are well predicted by all the three models. Some under-predictions can be observed for the prediction of the second peak, indicating that the interaction between co-flow and air stream is under-estimated. At 120 mm axial location, the PaSR model over-predicts the peak value by 13% while LFR model under-predicts by 24%.

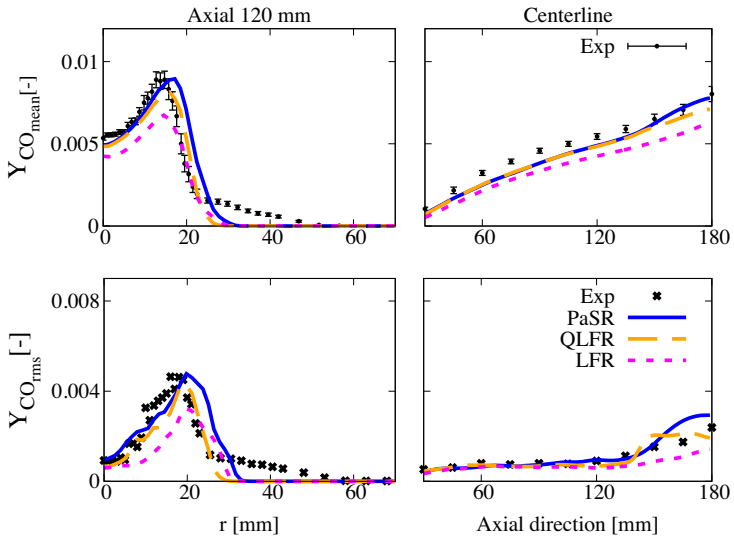

Fig. 9. Mean and root-mean-square (rms) CO mass fraction profile obtained with the conventional PaSR model, the PaSR based QLFR model and the LFR model, at two sampling locations (centerline and z = 120 mm), compared with the experimental measurements. Kinetic mechanism: KEE58.

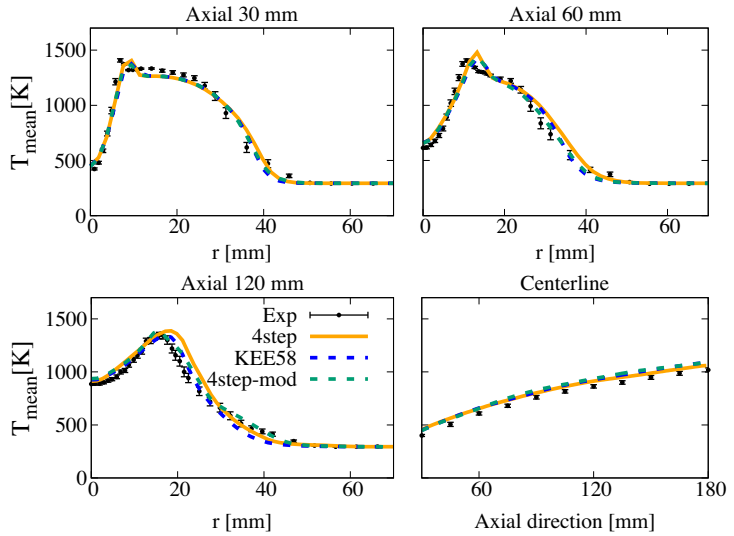

Fig. 10. Mean temperature profiles obtained with the conventional PaSR model using global mechanisms and a skeletal mechanism, at several sampling locations, compared to the experimental measurements.

The QLFR model predicts the peak value better than the previous two models, showing an under-prediction of 8%.

The mean and rms of species mass fraction of the oxidizer and products are shown in Figs. 7–9 as well. All models show good agreement with the experimental data at 120 mm axial location for the mean O_2 and H_2O profiles (Fig. 7). A slight shift of the peak value is observed at 60 mm for the mean H_2O profile, when using the PaSR approach. As far as the O_2 and H_2O rms values are concerned (Fig. 8), some under-predictions are observed at z = 60 mm, although the qualitative trend is well captured. At z = 120 mm, the QLFR model well captures the H_2O rms peak value, while PaSR and LFR models over-predict and under-predict the experimental peak value by 11 % and 18.5 %, respectively.

The CO mass fraction distribution is generally hard to capture in the AJHC system [12], because

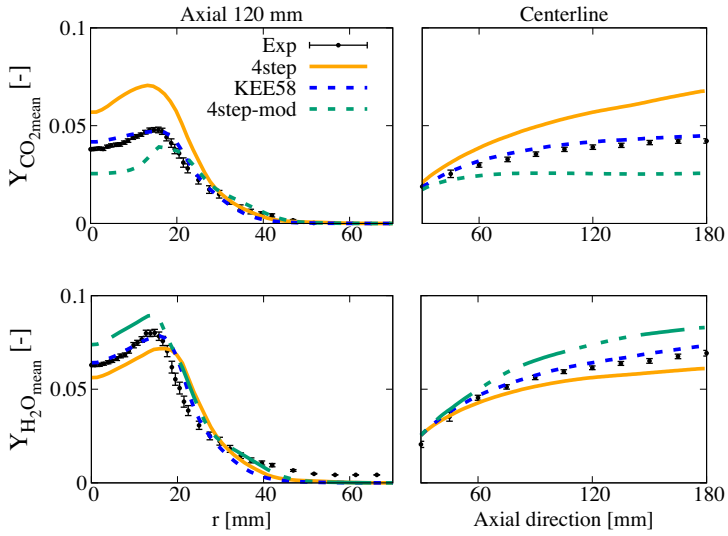

Fig. 11. Mean CO_2 and H_2O mass fraction profiles obtained with the conventional PaSR model using global mechanisms and a skeletal mechanism, at two sampling locations (z = 120 mm and centerline), compared to the experimental measurements.

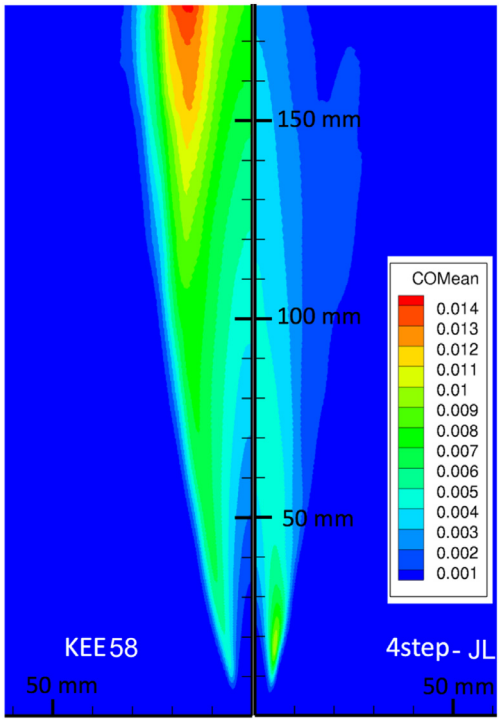

Fig. 12. Contour plot of mean CO mass fraction profile obtained using a skeletal (left) and a global (right) chemical mechanism.

the hot and diluted conditions modify the CO/CO_2 conversion rates [27]. In Fig. 9, both the mean and rms value of CO are presented. The PaSR model well predicts the mean and variance peak value at z = 120 mm and the centerline profile, except for the variance, when z ≥ 150 mm. The QLFR model provides results very close to PaSR, thus confirming the validity of the hypothesis $\kappa = 1$. The LFR model underestimates the mean CO peak value by 17 % at z = 120 mm, as well as the centerline profile. The CO profiles obtained from LFR model confirm that using this approach leads to an under-estimation of the intensity of turbulence/chemistry interactions with respect to the other two models.

4.2. Detailed versus global chemistry

To investigate the relevance of the kinetic mechanism on the results, two global 4-step mechanisms are benchmarked against the KEE58 mechanism in Fig. 10, using the conventional PaSR model. In Fig. 10, 4step denotes the original JL mechanism [24], 4step-mod represents the modified JL mechanism from Wang et al. [25] and KEE58 indicates the KEE mechanism [26].

The original JL mechanism provides acceptable predictions of the temperature field, although slight over predictions are observed for the mean radial temperature profiles at both z = 60 mm and z = 120 mm, by 45 K and 74 K, respectively. The modified JL mechanism, optimised for MILD combustion, is able to correct the over-prediced temperature peak from the original one, showing results closer to that obtained with the KEE58 mechanism. However, the main advantage associated to the use of more detailed mechanism can be observed when looking at the product mass fraction profiles. In Fig. 11, the centerline and downstream (120 mm) radial profiles of CO_2 and H_2O

mean species mass fraction are compared to the experimental data. It can be appreciated how the use of the original JL mechanism leads to a significant over-prediction of the mean CO_2 mass fraction while under-predicting H_2O levels. On the opposite, the modified JL mechanism provides a strong under-prediction of the mean CO_2 values and over-predicting H_2O mass fraction.

To further compare the global and skeletal mechanisms, Fig. 12 presents the contour plot of mean CO mass fraction, as provided by the KEE58 (left) and the original JL (right) mechanisms, respectively. Figure 12 clearly shows that the global scheme indicates a very fast CO/CO_2 conversion and fails to predict any CO formation downstream of the flame, thus leading to the over-estimation of CO_2 levels observed in Fig. 11.

5. Conclusions

In the present work, Large Eddy Simulations of the AJHC burner were carried out with the purpose of investigating the applicability of implicit combustion models in MILD combustion. Two implicit combustion models, QLFR and LFR, were benchmarked against the PaSR approach for turbulence/chemistry interactions. Two 4-step global mechanisms and a skeletal mechanism were used. The conclusion can be summarized as follow:

- The reaction regions are characterised by large values of κ (close to 1.0) and low Damköhler number (≤ 0.15), indicating that combustion occurs under distributed conditions.
- Among the two implicit combustion models, the QLFR model provides results that are very close to the PaSR model, thus confirming that κ values are close to 1.0 in MILD combustion. The LFR model generally under-predicts the level of turbulence/chemistry interactions in the flame. However, it correctly reproduces the centerline mean temperature and species profiles.
- Global mechanisms cannot faithfully predict the main products mass fractions, confirming the need of finite rate chemistry in MILD combustion.

The numerical results justify the application of implicit closures in the context of MILD combustion. The choice between the different approaches investigated here in realistic configurations will depend on the local *Da* and *Re* numbers, as well as on the size of the chemical mechanism employed.

Acknowledgments

This project has received funding from the European Union's Horizon 2020 research and innovation program under the Marie Skłodowska-Curie grant agreement No. 643134. The research of the last author was sponsored by the European Research Council, Starting Grant No. 714605.

Supplementary material

Supplementary material associated with this article can be found, in the online version, at doi:10.1016/j.proci.2018.09.033.

References

[1] J.A. Wünning, J.G. Wünning, *Prog. Energy Combust. Sci.* 23 (1997) 81–94.
[2] A. Cavaliere, M. de Joannon, *Prog. Energy Combust. Sci.* 30 (2004) 329–366.
[3] Y. Minamoto, N. Swaminathan, R.S. Cant, T. Leung, *Combust. Sci. Technol.* 186 (8) (2014) 1075–1096.
[4] Y. Minamoto, N. Swaminathan, *Proc. Combust. Inst.* 35 (3) (2015) 3529–3536.
[5] J. Chomiak, *Combustion: A Study in Theory, Fact and Application*, Abacus Press/Gorden and Breach Science Publishers, New York, 1990.
[6] C. Duwig, P. Iudiciani, *Fuel* 123 (2014) 256–273.
[7] B.B. Dally, A.N. Karpetis, R.S. Barlow, *Proc. Combust. Inst.* 29 (2002) 1147–1154.
[8] J. Aminian, C. Galletti, S. Shahhosseini, L. Tognotti, *Flow Turbul. Combust.* 88 (4) (2012) 597–623.
[9] M.J. Evans, P.R. Medwell, Z.F. Tian, *Combust. Sci. Technol.* 187 (7) (2015) 1093–1109.
[10] A. Parente, M.R. Malik, F. Contino, A. Cuoci, B.B. Dally, *Fuel* 163 (2015) 98–111.
[11] M. Ihme, Y.C. See, *Proc. Combust. Inst.* 33 (1) (2011) 1309–1317.
[12] M. Ihme, J. Zhang, G. He, B. Dally, *Flow Turbul. Combust.* 89 (2012) 449–464.
[13] Y. Afarin, S. Tabejamaat, A. Mardani, Large eddy simulation study of H2/CH4 flame structure at MILD condition, in: Seventh Mediterranean Combustion Symposium, 2011. Naples, Italy.
[14] A. Cuoci, A. Frassoldati, T. Faravelli, E. Ranzi, *Comput. Phys. Commun.* 192 (2015) 237–264.
[15] A. Yoshizawa, K. Horiuti, *J. Phys. Soc. Jpn.* 54 (1985) 2834–2839.
[16] S. Huang, Q.S. Li, *Int. J. Numer. Methods Eng.* 81 (2010) 835–865.
[17] F. P. Kärrholm, Numerical Modelling of Diesel Spray Injection, Turbulence Interaction and Combustion, (Ph.D. thesis), Chalmers University of Technology, Chalmers, Sweden, 2008.
[18] V. Sabelnikov, C. Fureby, *Progr. Propuls. Phys.* 4 (2013) 539–568.
[19] C. Fureby, Comparison of flamelet and finite rate chemistry LES for premixed turbulent combustion, in: 45th AIAA Aerospace Sciences Meeting and Exhibit, American Institute of Aeronautics and Astronautics, 2007.
[20] C. Duwig, K.J. Nogenmyr, C.K. Chan, M.J. Dunn, *Combust. Theor. Model.* 15 (4) (2011) 537–568.
[21] Z. Gao, C. Jiang, C.H. Lee, *Int. J. Hydrogen Energy* 41 (30) (2016) 13238–13253.
[22] N. Kornev, H. Kröger, E. Hassel, *Commun. Numer. Meth. Eng.* 24 (2008) 875–877.

[23] T.J. Poinsot, S.K. Lele, *J. Comput. Phys.* 101 (1) (1993) 104–129.
[24] W.P. Jones, R.P. Lindstedt, *Combust. Flame* 73 (1988) 233–249.
[25] L. Wang, Z. Liu, S. Chen, C. Zheng, *Combust. Sci. Technol.* 184 (2) (2012) 259–276.
[26] R.W. Bilger, S.H. Stårner, R.J. KEE, *Combust. Flame* 80 (2) (1990) 135–149.
[27] J. Andersen, C.L. Rasmussen, T. Giselsson, P. Glarborg, *Energy Fuels* 23 (2009) 1379–1389.